Atomic motions in the crystalline $Al_{50}Cu_{35}Ni_{15}$ alloy

2000 J. Phys.: Condens. Matter 12 4021

(http://iopscience.iop.org/0953-8984/12/17/309)

J. Phys.: Condens. Matter **12** (2000) 4021–4041. Printed in the UK PII: S0953-8984(00)09088-3

Atomic motions in the crystalline $Al_{50}Cu_{35}Ni_{15}$ alloy

U Dahlborg†, W S Howells‡, M Calvo-Dahlborg† and J M Dubois†

† LSG2M-UMR 7584, CNRS-INPL, Centre d'Ingènièrie des Matériaux, Ecole des Mines, Parc de Saurupt, 54042 Nancy, France

‡ Rutherford Appleton Laboratory, Chilton, Didcot, Oxon, OX11 0QX, UK

Received 29 October 1999

Abstract. This paper describes quasi-elastic neutron scattering experiments on the $Al_{50}Cu_{35}Ni_{15}$ alloy performed on the IRIS spectrometer at ISIS, Rutherford Appleton Laboratory, and on the MIBEMOL spectrometer at Laboratoire Léon Brillouin, Saclay. The aim was to investigate if atomic hopping motions are restricted only to occur in systems with quasicrystalline local order. It is found that frequent jumps of Cu and Ni atoms between different interstitial lattice positions on the time scale 1 to 100 ps are taking place in this alloy at high temperature. This is the same time scale that has been found earlier in quasicrystals and it suggests that this kind of motion is likely to take place in any metallic alloy at high temperature and that it is not a special property of quasicrystals.

1. Introduction

In crystalline solids the atoms occupy well defined equilibrium positions. However, the presence of defects in the crystalline lattice makes it possible for atoms to move. Several different mechanisms have been found responsible for this ability. In metals and alloys close to the melting point, where the vacancy concentration is of the order of 10^{-4}, the main mechanism is jumps to nearest-neighbour sites but also, to some extent, to next-nearest-neighbour sites [1, 2]. Usually the diffusion coefficient obeys an Arrhenius law but in some cases, mainly for bcc structures, the Arrhenius plots show an upward curvature, which indicates that several different mechanisms, are at work. The experimental studies of the diffusion mechanisms in crystal lattices have been mainly done by neutron quasielastic scattering because it can yield accurate microscopic information both on the geometry and the time scale of the atomic jump motion [3]. An excellent review of the diffusion phenomenon in metals and alloys has recently been published [4].

In recent years extensive experimental investigations of the structure and dynamics of quasiperiodic alloys or quasicrystals (QC) and their approximants have been carried out. The details of the elementary excitations in QC materials are considerably different from those in periodic systems. One reason is the fundamental aperiodicity of these structures and, as a consequence, the concept of the Brillouin zone is ill defined. The aperiodicity implies the existence of additional dynamical excitations, either collective (phason modes) or individual (phason flips). These are, in this context, to be considered as defects that occur when the quasicrystalline matching rules are not fulfilled. Phasons are accordingly to be associated with an atomic motion of diffusive nature. A scheme for atomic transport in quasicrystals which is a combination of the basic mechanism in ordinary materials, i.e. moving vacancies, and of atomic jumps in a double-well potential, was devised by Kalugin and Katz [5]. It should be

0953-8984/00/174021+21$30.00

emphasized that the existence of dynamical phasons has been a key issue for the description of the properties of quasicrystals.

Recently, the first evidence for atomic hopping at high temperature in a quasicrystalline structure, a perfect icosahedral quasicrystal of composition $Al_{62}Fe_{25.5}Cu_{12.5}$, was found by using the neutron quasielastic scattering technique [6]. Using the isotope substitution technique it was possible to conclude that the observed quasi-elastic scattering component was originating from the motion of Cu atoms on a picosecond time scale and that this motion was confined in space. Later, measurements by Mössbauer spectroscopy and the neutron back-scattering technique have shown that Fe atoms perform a hopping motion as well but at a much slower time scale (nanosecond) than that of Cu atoms [7, 8]. Later, hopping of Mn atoms at high temperature was shown to also take place in the AlPdMn system [9]. A comprehensive review of these results and their interpretation has recently been presented [10]. Hopping of Al atoms in the sub-kHz range at low and very low temperatures has also been found by applying the NMR technique on the quasicrystalline system $Al_{70}Pd_{21.4}Re_{8.6}$ [11].

Some work has also been carried out on parent crystalline phases of quasicrystals. Experiments performed on the cubic β-phase of $Al_{50}Fe_{25}Cu_{25}$ [6] did not give any evidence for atomic hopping while the quasi-elastic neutron signal was found to be the same in rhombohedral and icosahedral phases of $Al_{62.5}Cu_{26.5}Fe_{11}$, showing that atomic hopping is taking place in this approximant (see for example [10]). This is a particularly important result because the hysteresis of the reversible rhombohedral-to-icosahedral transition allowed the two measurements to be performed at the same temperature.

In this report the neutron scattering technique has been used to investigate the atomic dynamics in the $Al_{50}Cu_{35}Ni_{15}$ alloy. In the long-range ordered structures of the Al_x-$(Cu,Ni)_{1-x}$ system, designated as t phases, the Al atoms form a primitive rhombohedrally deformed cubic lattice while in the cube centres Cu/Ni atoms and vacancies form a pseudo-binary system along the (111) axis [12, 13]. It was later pointed out that the number of layers in the different τ phases form a Fibonacci sequence, thus indicating the close resemblance between the vacancy ordered bcc and the quasicrystalline structures [14]. The AlCuNi alloy can thus be considered as a one-dimensional quasicrystal. The structural similarity between the CsCl and the decagonal quasicrystalline phases has also been suggested from positron annihilation measurements (PAM) on several materials of both kinds [15]. Furthermore, these experiments showed the presence of free volumes of the size of a lattice vacancy in the CsCl structure. It should be mentioned that PAM has also indicated that a high density of vacancy type structural defects exists in the AlPdMn icosahedral quasicrystal [16]. In addition, radiotracer measurements in combination with serial sectioning of AlPdMn quasicrystalline samples have shown that the diffusion is not significantly different from those in related crystalline materials [17, 18]. The aim of the present study is thus to investigate if atomic hopping at a large rate is restricted to taking place in systems with quasicrystalline local order or if it exists more generally in metallic alloys at high temperatures.

2. Experimental details and sample characterization

Three series of measurements have been performed on the backscattering spectrometer IRIS at the ISIS neutron spallation source, Rutherford Appleton Laboratory (RAL), UK. The wavelength of the neutrons was in all cases 6.6 Å and the energy resolution about 15 μeV. Neutron energy transfers E in the range -0.4 to 0.4 meV were covered. The angular span of the 50 detector elements utilizing the 002 reflection from pyrolytic graphite for energy analysis of the scattered neutron ranges from 25 to 155 degrees. Thus, momentum transfers Q in the range $0.5 < Q < 1.84$ Å^{-1} could be covered. In order to improve the statistics, the measured

spectra were merged into groups of 5 (except for the group at the lowest Q which because of large background, only contained spectra from two detectors), yielding a Q resolution varying from about 0.2 $Å^{-1}$ at the smallest Q to about 0.05 $Å^{-1}$ at the largest Q.

One set of measurements was performed on the MIBEMOL time-of-flight spectrometer at Laboratoire Léon Brillouin, Saclay, France. The wavelength of the incident neutrons was 5 Å and spectra were recorded in 72 detectors at scattering angles between 26 and 142 degrees. This implies that a Q range from about 0.6 to about 2.4 $Å^{-1}$ was covered. The energy resolution was about 0.18 meV. In order to obtain spectra with good statistical accuracy only two samples were investigated, the one containing natural elements and the one with 'null scattering' nickel. Spectra were recorded at the same temperatures as were measured in the second series of measurements on IRIS, 570 °C and 920 °C. The intensities recorded in the 72 detectors were merged into 10 spectra, ranging in Q from about 0.5 to about 2.4 $Å^{-1}$. However, with respect to elastic intensities the statistical accuracy was sufficient for use of spectra measured in single detectors.

The powder samples of nominal composition $Al_{50}Cu_{35}Ni_{15}$ were contained in 5 cm high cylinders of single-crystalline sapphire with an outer diameter of 7 mm and a wall thickness of 0.5 mm. The alloys were produced by cold pot melting and coarsely ground. The masses of the samples were in the range 3 to 4 g yielding an average transmission larger than 95%. The c-axis of the sapphire was in the direction of the cylinder axis (perpendicular to the neutron beam) which made it possible to avoid any Bragg scattering originating from the container. It should be mentioned that before recording every spectrum checks were performed to establish that no Bragg peak from the sapphire could be seen. As a matter of fact, out of more than 15 individual measurements it was only once that the container had to be rotated to avoid any Bragg scattering in the covered range of scattering angles. The sapphire container was held in a thin-walled tube of Nb attached to a centre stick in a furnace. No Bragg scattering from niobium is possible because of the large neutron wavelength used. In the first series of measurements on IRIS a sample of natural composition was studied in 50 degree intervals from room temperature up to 950 °C. In the second and third series three samples were investigated, one containing natural elements (denoted below as the n–n–n sample), one containing natural Al and Cu and 'null matrix' Ni (denoted below as the n–n–0 sample), and a third one containing natural Al, the copper-65 isotope and 'null matrix' Ni (denoted below as the n–65–0 sample). The 'null matrix' Ni was achieved by mixing the nickel-60 and nickel-62 isotopes in a ratio such that the scattering length for coherent scattering was zero. In order to study the temperature dependence spectra of scattered neutrons were recorded at 570 and 920 °C in the second series of measurements while in the third series spectra were recorded only at 920 °C. On MIBEMOL only two samples, the one with natural composition (n–n–n) and the one with 'null matrix' Ni (n–n–0), were studied both at 570 and 920 °C. In all measurements the same samples have been used.

Table 1. Contributions to the total scattering cross sections of the three investigated samples. The absorption cross sections are given for a neutron wavelength of 1.8 Å.

	Coherent contributions: α_{ij}						Total cross sections per scattering unit		
Sample	Al–Al	Cu–Cu	Ni–Ni	Al–Cu	Al–Ni	Cu–Ni	Coherent	Incoherent	Absorption
$^{N}Al^{N}Cu^{N}Ni$	0.374	0.917	0.300	1.170	0.670	1.049	4.48	1.86	2.11
$^{N}Al^{N}Cu^{0}Ni$	0.374	0.917	0	1.170	0	0	2.46	1.56	2.30
$^{N}Al^{65}Cu^{0}i$	0.374	1.733	0	1.610	0	0	3.72	2.57	1.74

The measured quasielastic spectra were corrected for empty container scattering (measured at the appropriate temperature) and normalized to absolute cross section units via a vanadium calibration measurement. Multiple scattering was considered to be small because of the large neutron transmission of all samples together with the relatively large absorption cross section (compare table 1). All spectra have been divided by the sample mass in order to facilitate intensity comparisons.

3. Theoretical background

The total dynamic scattering function $S_{tot}(Q, E)$ per atom for a multi-component alloy can generally be written as

$$\sigma S(Q, E) = \sum_{i,j}^{n} \alpha_{ij} S_{ij}(Q, E) + \sum_{i}^{n} \beta_i S_i^{inc}(Q, E) \tag{1}$$

where i, j represent the component atoms and n is the number of different kinds of atoms in the alloy. $S_{ij}(Q, E)$ and $S_i^{inc}(Q, E)$ are the partial coherent and the incoherent scattering functions, respectively, and α_{ij} and β_i are weight factors for the partial scattering functions. These are given by $\alpha_{ij} = 4\pi c_i c_j b_i b_j$ and $\beta_i = c_i \sigma_i^{inc}$, with c_i and b_i being the concentration and the bound atom scattering length of atom i, respectively. σ_i^{inc} is the incoherent scattering cross section for atom i and σ is the total scattering cross section for the alloy

$$\sigma = 4\pi \sum_{i,j}^{n} c_i c_j b_i b_j + \sum_{i}^{n} c_i \sigma_i^{inc}. \tag{2}$$

The α_{ij} factors and the total coherent, incoherent and absorption cross sections are given in table 1.

4. Crystalline structure

The presence of decagonal quasicrystals in the AlCuNi system around the relative composition 65–20–15 has been reported in [19, 20]. However, the decagonal phase has always been found to coexist with the vacancy ordered bcc CsCl phase. In order to obtain a sample as close as possible to a single phase, alloys of several compositions were produced and investigated by x-ray diffraction and differential scanning calorimetry. From these investigations the $Al_{50}Cu_{35}Ni_{15}$ alloy was found to be the one most suitable for further studies.

In order to determine the structure of the samples two sets of high-resolution neutron diffraction measurements were performed on the LAD diffractometer, also at the ISIS neutron spallation source. One set of measurements aimed at checking the structure of the three samples to be used on IRIS and the other set aimed at following the structural changes in a sample consisting of natural elements in the temperature interval 20 °C $< T <$ 1000 °C. The diffraction patterns, obtained at 20 °C, of the three IRIS samples are shown in figure 1(a). The peaks can be indexed according to a bcc structure with a lattice constant of 4.122 ± 0.002 Å. There are, however, some very weak intensity lines which might indicate that the alloy is not a single phase or that a superstructure exists in the alloy at 20 °C. Apart from the differences between the three patterns due to the isotope substitution, there are some small differences but these are believed to have a negligible influence on the results presented below. The diffraction patterns measured at different temperatures for the sample consisting of natural elements are shown in figure 1(b). The small difference between the two patterns for the *n–n–n* sample in figures 1(a) and 1(b), (see the peak at 1.6 Å^{-1}) stems from the two facts that the patterns were

recorded at different occasions and that this sample is not completely polycrystalline and thus not completely isotropic. The alloy passes through another phase in the temperature region 500 to 600 °C. Above this temperature the alloy seems to consist of only one phase which is in accordance with earlier investigations [20]. A complete structural analysis is under way. It should be mentioned that according to [21] the solidus of the alloy is at about 1150 °C and the liquidus at about 1400 °C. Accordingly, during all measurements the samples have been in the solid phase which has also been confirmed by differential scanning calorimetry measurements.

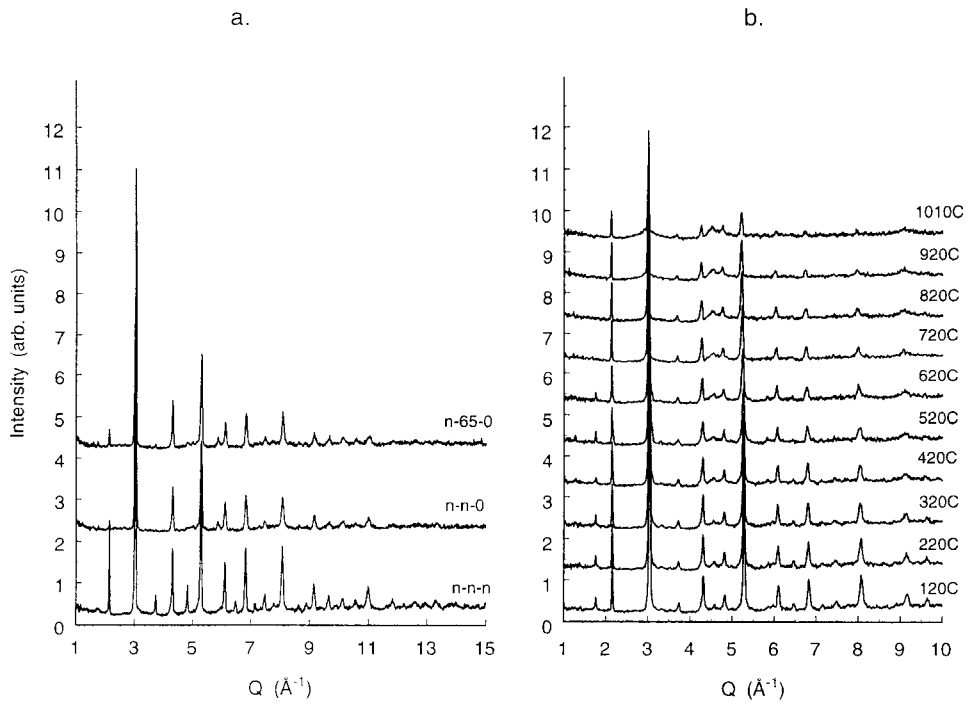

Figure 1. (a) Diffraction patterns measured at room temperature for the three investigated samples. The patterns from the *n*–*n*–0 and *n*–65–0 samples have been shifted +2 and +4 intensity units, respectively. (b) Diffraction patterns, each displaced +1 intensity unit relative to the one at the preceeding temperature, at the different indicated temperatures for the *n*–*n*-*n* sample.

As can be seen in figure 1(b) all Bragg peaks remain sharp with a width given by the instrumental resolution ($\Delta Q/Q \approx 1.2\%$) even at the highest temperature with the exception of a small feature at about 4.6 Å^{-1}. However, at the foot of the (200) Bragg peak at $Q = 3.06$ Å^{-1}, and it seems only at this peak, a diffuse scattering component starts to be visible at about 700 °C and grows with increasing temperature. The intensity of such a diffuse component close to Bragg peaks (the so-called Huang scattering) gives information about the presence of point defects [22]. As the Debye–Waller factor for AlCuNi is small, it can be concluded that the distortion of crystalline lattice created by the defects is small but long-ranged. The magnitude of the scattering intensity is in such a case determined by the elastic constants of the crystal and the force dipole tensor [22]. According to theory the intensity should vary as $(\boldsymbol{Q} - \boldsymbol{G})^{-2}$ when $\boldsymbol{Q}$ approaches the reciprocal lattice vector $\boldsymbol{G}$. This is in agreement with the experimental observation. In order to quantify the magnitude of the distortion the shape of the diffuse intensity was approximated by a Lorentzian function centred at the reciprocal lattice point.

The width of the fitted Lorentzian was in all cases found to be the same within the fitting errors and considerably smaller than the Q resolution which gives confidence in the procedure. The area of the Lorentzian function is shown in figure 2. At temperatures where two points can be seen one corresponds to the heating cycle (circles) and the other to the cooling cycle (triangles). Assuming that the measured diffuse intensity is governed by an Arrhenius law, an activation energy of 0.60 ± 0.04 eV is obtained (the full curve in figure 2). This value is close both to the activation enthalpy for single-vacancy formation and for atomic migration in pure aluminium but considerably smaller than in pure nickel and copper (see table 2). However, it is twice as high as those calculated for other bcc structures at high temperature (β-Ti, β-Zr, β-Hf) (see [25] for details).

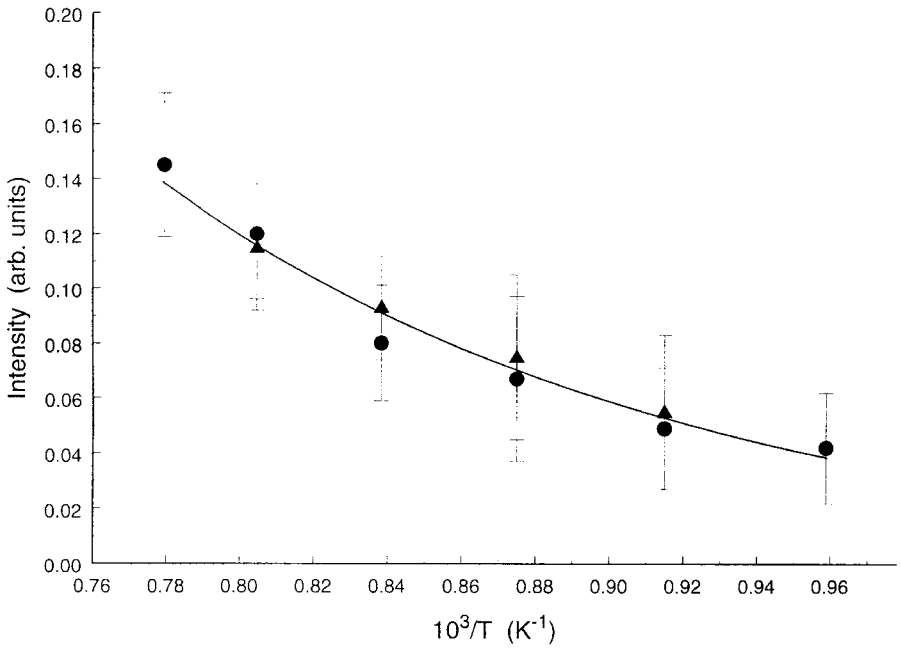

Figure 2. The temperature dependence of diffuse scattering intensity at the foot of the (200) diffraction peak during heating (circles) and subsequent cooling (triangles) of the *n–n–n* sample. The full line is a fit of an exponential function to the measured points.

Table 2. Some data for the pure elements in the $Al_{50}Cu_{35}Ni_{15}$ alloy.

Element	Atomic radius in a 12 coordination environment [23] (Å)	Activation enthalpy of single-vacancy formation in pure element [24] (eV)	Activation energy of atomic migration in pure element [24] (eV)
Al	1.432	0.67 ± 0.03	0.61 ± 0.03
Ni	1.246	1.79 ± 0.05	1.04 ± 0.04
Cu	1.278	1.28 ± 0.05	0.70 ± 0.02

5. Results from the high resolution measurements on the IRIS spectrometer

One example of a measured spectrum from the sample containing 'null matrix' Ni and ^{65}Cu and held at 920 °C is shown in figure 3. The broken line is the resolution function, as given by the vanadium calibration run. It is obvious that there is a small but significant extra intensity contribution at the foot of the measured spectrum indicating the existence of a quasielastic scattering component. In order to isolate this, it was decided to apply a Bayesian method of analysis [26] available for users on IRIS. One of the advantages in using the Bayesian method of analysis is that it is completely unbiased and thus, no feature which is not in the data can be extracted from them. As the quasielastic scattering component is small and the statistical noise of considerable amplitude, it was also decided not to try to make any line shape analysis but to just assume that the quasielastic scattering can be described by one single Lorentzian function.

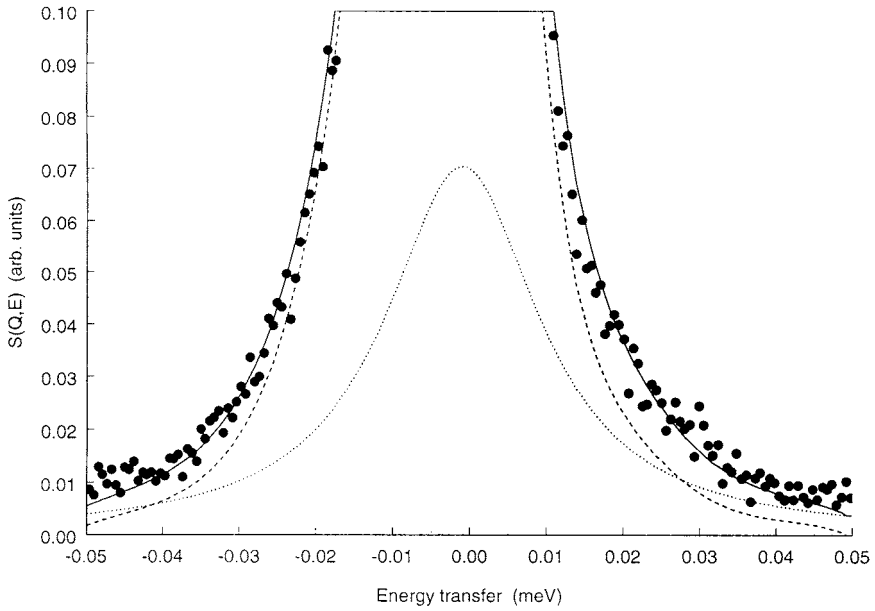

Figure 3. The quasielastic spectrum in the near elastic energy region from the *n–n–*0 sample at 920 °C measured on the IRIS spectrometer. The broken line shows the resolution function normalized to peak maximum and the full line the fitted sum of one elastic and one quasielastic contribution of Lorentzian shape, convoluted with the resolution function according to equation (3). The dotted line shows the quasielastic component. The phonon background is very small and it is not visible in the scale of the figure.

From these general considerations the measured spectra were, assuming that Q is constant over the covered energy transfer range at one scattering angle, described by an expression of the type

$$S(Q, E) = C[A_0\delta(E) + \sum_{j=1}^{N} \frac{A_j}{\pi} \frac{W_j}{E^2 + W^2} + B(E)] \otimes R(E) + N(E) \qquad (3)$$

where C is a coupling constant, E the neutron energy transfer, A_j and W_j are amplitudes and half widths at half height of the different scattering contributions, respectively, $R(E)$ the resolution function, $B(E)$ a background of inelastic scattering and $N(E)$ the statistical noise.

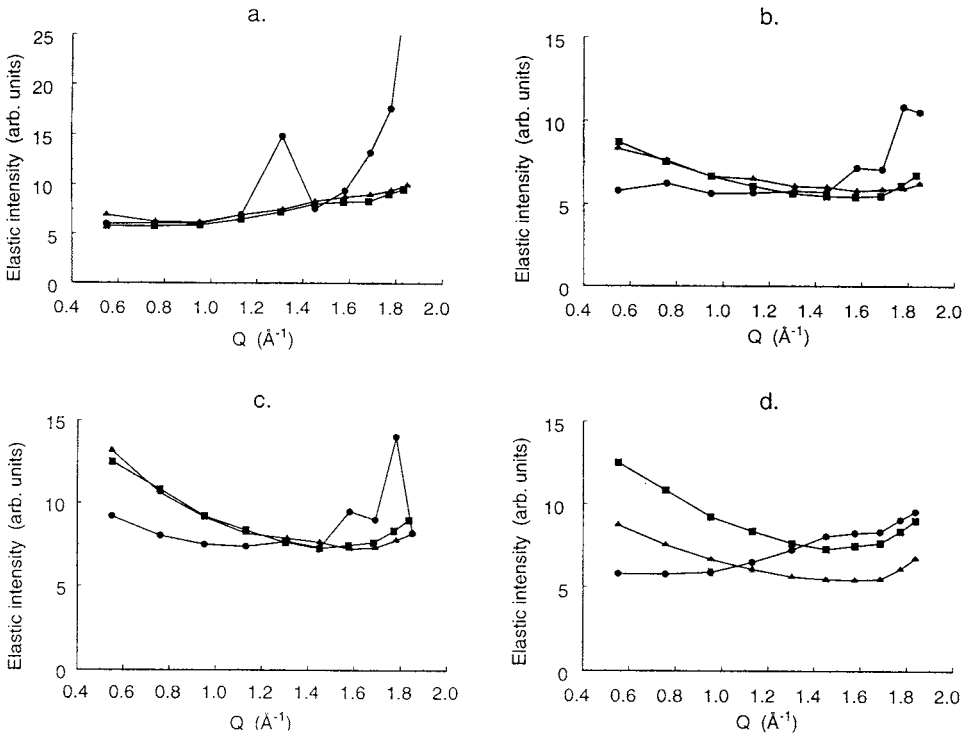

Figure 4. Elastic intensities measured at 920 °C on the IRIS spectrometer. Filled circles: 570 °C, triangles: 920 °C (second series), filled squares: 920 °C (third series). (a) *n*–*n*–*n* sample, (b) *n*–*n*–0 sample, (c) *n*–65–0 sample. (d) Total intensity of the elastic peak from the third series of measurements on IRIS. Filled circles: *n*–*n*–*n* sample, triangles: *n*–*n*–0 sample, filled squares: *n*–65–0 sample. The curves are included to guide the eye.

$\otimes$ denotes convolution. As can be seen in figure 3 (full curve), a very good agreement between experiment and calculation is obtained by this procedure, giving support to the interpretation that the measured spectrum is consisting of two components, one elastic and one quasielastic component (broken and dotted curves, respectively). There is a small difference between the measured spectrum and the fitted curve in the wings, which might indicate the presence of another intensity component. However, the statistics are not good enough for a definite conclusion. It should be mentioned that in no case was it possible to describe the entire quasielastic spectrum by a curve constructed only by a convolution of a single Lorentzian and the resolution function, i.e. without a strictly elastic scattering component.

The intensities integrated within the resolution window, i.e. the elastic scattering components, at 570 °C and 920 °C for the different measurements are shown in figure 4 while the total intensity and the width of the quasielastic component, obtained from an analysis according to equation (3) of the third series of measurements on IRIS, are shown in figure 5. For comparative reasons figure 4(d) displays the elastic intensities measured for the three samples in the third series of measurements. For the 570 °C data and for Q less that 0.9 Å^{-1} for the 920 °C data, it was not possible to isolate a quasielastic component with reasonable confidence. Several qualitative remarks can be made:

- The results from the different sets of measurements are reproducible and consistent. Both

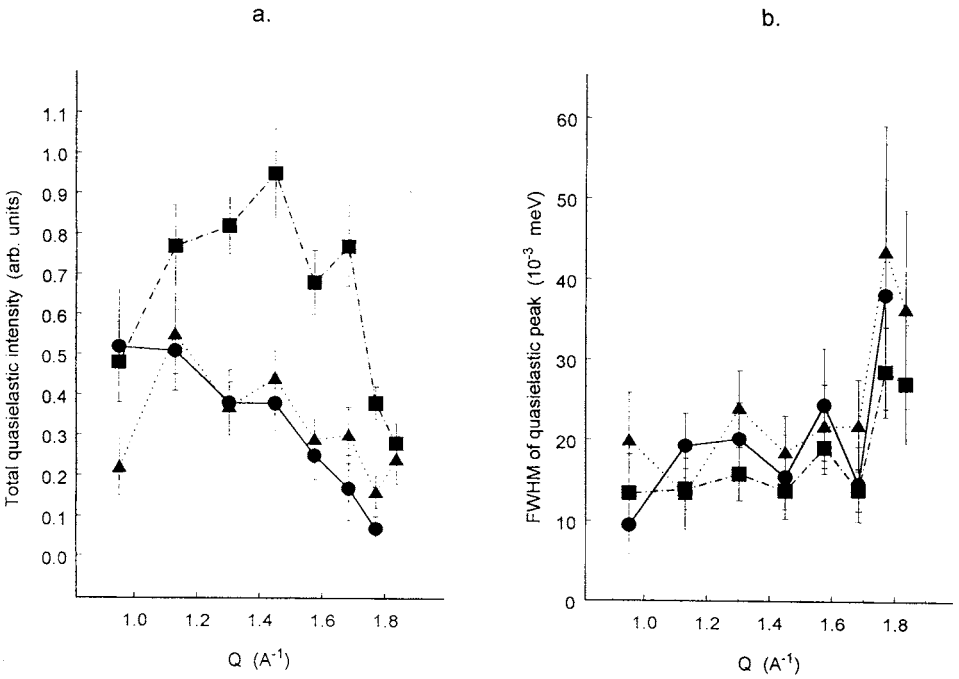

Figure 5. (a) Intensity and (b) full width at half maximum (FWHM) of the quasielastic peak at 920 °C from the third series of measurements on IRIS. Circles: *n*–*n*–*n* sample; triangles: *n*–*n*–0 sample; squares: *n*–65–0 sample. The lines are included to guide the eye. The resolution of IRIS is about 15 μeV.

these facts indicate that no annealing effects occur in the samples after repeated heating.

- The structure of all samples at 570 °C is different from the structure at 920 °C and that agrees with the results from the diffraction measurements.
- The elastic intensity for the isotope containing samples varies in a smooth manner with Q and its magnitude increases with temperature. There are no obvious signs of Bragg peaks, even in single detectors, at Q values other than those found in the diffraction measurements (see figure 1).
- The elastic intensity from the sample of natural composition does not vary significantly with temperature except at Q values where neighbouring Bragg peaks have an influence (around $Q = 1.3$ Å^{-1} and for large Q).
- In view of the cross section values given in table 1, the elastic intensity is lower than expected for the sample of natural element composition.
- The Q variation of the quasielastic intensity component is different for *n*–*n*–*n* samples compared to the isotope containing ones.
- The width of the quasielastic peak is, within the error bars, the same for all samples and is constant for Q values less than about 1.7 Å^{-1} above which it increases.

When comparing intensities from the different samples it has to be stressed that if a superstructure exists in the alloys, a coherent contribution may appear in the Q range of figure 4(a) and this would make any comparison of elastic intensities meaningless. However, as mentioned above, no signs of Bragg peaks supporting the existence of a superstructure at 920 °C were seen in the diffraction measurements.

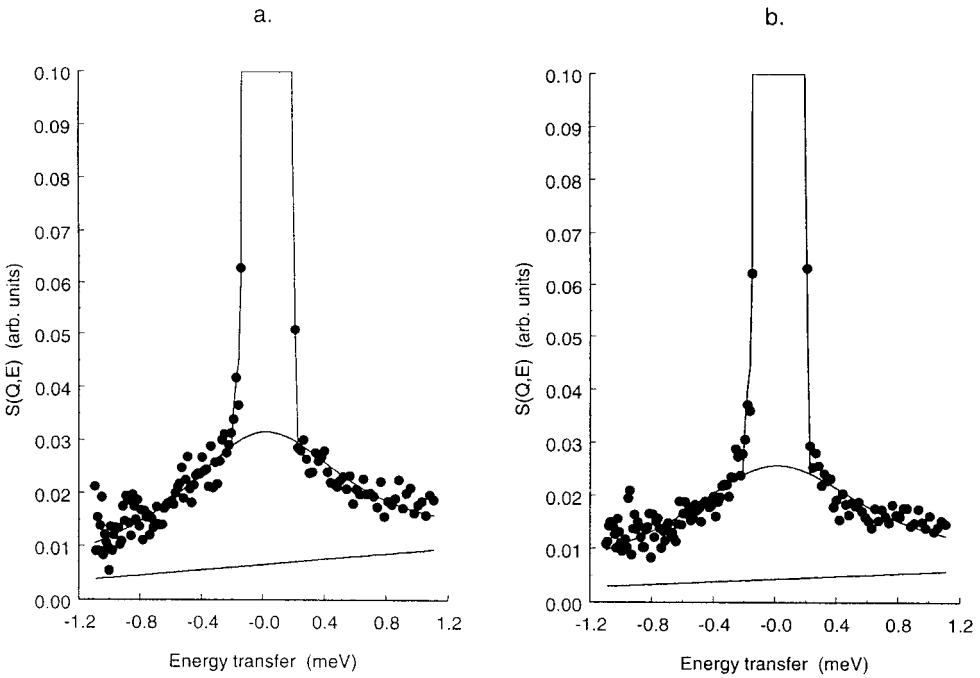

Figure 6. Spectra in the near elastic energy region measured on the MIBEMOL spectrometer in an enlarged scale for $Q = 2.01$ Å^{-1}. The different intensity components are shown as solid curves. (a) *n–n–n* sample, (b) *n–n–*0 sample.

The results presented in figures 4 and 5 exhibit several features, which cannot be interpreted directly. To take one example, why is the intensity from the *n–n–n* sample so low compared to the isotope containing ones? One possible explanation is that, at least, some Ni atoms are moving very fast, either by continuous or by jump diffusion, in the crystalline lattice. In this case these atoms will contribute to the quasielastic peak and not to the elastic one. This quasielastic peak will be very wide and, because of the very good resolution of the IRIS spectrometer, it will appear in the measured spectra as a flat background. It was in order to investigate this possibility that the measurements on the MIBEMOL spectrometer were performed.

6. Results from the measurements on the MIBEMOL spectrometer

In the MIBEMOL spectra a quasielastic scattering component could also be seen at 920 °C while it was absent at 570 °C. In order to separate the elastic and quasielastic scattering the spectra were fitted using a least squares method by an analytical expression consisting of a sum of three terms: the resolution function, which describes the elastic component, a convolution of a Lorentzian and the resolution function, which describes the quasielastic component, and a sloping linear background, which simulates the phonon background. In all cases good agreement between calculated and measured spectra could be obtained. However, some systematic differences between the fitted curves and measured data do exist which might indicate that the quasielastic scattering is not adequately described by a single Lorentzian function. The statistical accuracy of the data does though make a detailed line shape analysis

meaningless. Two examples of fitted curves are shown in figure 6.

The amplitudes of the elastic and the quasielastic scattering components as well as the width of the quasielastic peak, obtained from the fits, are shown in figure 7. It can be seen that the elastic intensity does not, apart from the Bragg peaks, vary much with temperature and that the quasielastic intensity at high temperature is very similar for the two samples while the width of the quasielastic peak is different.

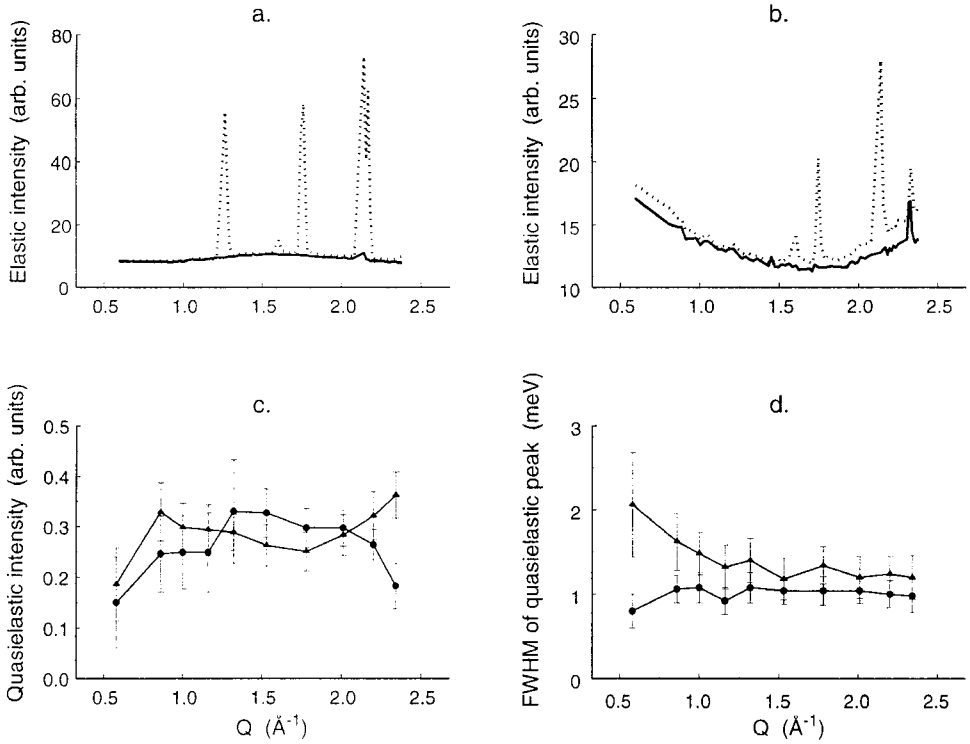

Figure 7. Results obtained from the fits of the MIBEMOL data. (a) Elastic intensities for the *n–n–n* sample. Dotted line: 570 °C, full line: 920 °C. (b) Elastic intensities for the *n–n–*0 sample. Dotted line: 570 °C, full line: 920 °C. (c) Total intensity and (d) FWHM of the quasielastic peak. Filled circles: *n–n–n* sample, triangles: *n–n–*0 sample. The curves are included to guide the eye. The experimental resolution was about 0.18 meV.

7. Discussion

7.1. Possible models to interpret the results

The variations of amplitude and width of the two scattering components exhibit several distinct features, which at first sight are not compatible. The existence of a quasielastic contribution shows that some kind of diffusive motion takes place in the alloy at high temperature. The diffuse scattering observed in the diffraction patterns also indicates that the crystalline lattice is distorted at high temperature and that the distortion field is asymmetric. Thus, in order to interpret the results presented in figures 4, 5 and 7, several different possibilities have to be considered. An important observation in this respect is that the quasielastic scattering component in all samples, when it exists, is small compared to the elastic one, only of the

order of a few percent. This indicates that only relatively few atoms are involved in the diffusion process. Two different kinds of diffusion processes can be identified: (a) diffusion in a restricted volume and (b) long-range diffusion. In the first case the derived scattering functions contain an elastic peak while in the second no strictly elastic scattering occurs. We give below a brief outline of the models, which might describe the obtained results. A full account of some of the models can be found in [3].

a. Diffusion in a restricted medium

(1) *Atoms are jumping back and forth between N energy equivalent lattice sites which are separated by a distance d*. No atomic transport is taking place but the sites make up a cluster of vacancies and/or interstitial sites. The scattering function per atom is for a powder given by [3]

$$S(Q, E) = \frac{1}{N}\mathrm{e}^{-2W}\left[(1 + (N-1)j_0(Qd))\delta(E) + (N-1)(1 - j_0(Qd))\frac{1}{\pi}\frac{\Gamma}{E^2 + \Gamma^2}\right] \qquad (4)$$

e^{-2W} is the Debye–Waller factor, j_0 is the spherical Bessel function of zero order and $G = h/2pt$, where t is the residence time in one position and h the Planck constant. The jump between the two sites is assumed to be instantaneous. If several jump distances are involved equation (4) will be more complicated but it will have a similar structure. Thus, a measured spectrum, according to this model, will exhibit an elastic peak whose amplitude is oscillating as a function of Q and a quasielastic peak whose amplitude varies with Q while the width shows no Q dependence. Several jump directions and lengths, implying a Q dependent t, may exist but in the present case of a polycrystalline sample this effect will, to a large extent, be averaged out and not possible to detect. This model thus agrees qualitatively with the experimental results.

(2) *Atoms are jumping between two non-equivalent sites.* In this case the scattering function may formally be written as [3]

$$S(Q, E) = [1 - C(1 - j_0(Qd)]\delta(E) + C[1 - j_0(Qd)]\frac{1}{\pi}\frac{\gamma}{E^2 + \gamma^2} \qquad (5)$$

where C and γ are constants depending on the residence times of an atom in the two sites. This model has been further developed in terms of phonon-assisted hopping [10] and it has satisfactorily explained the temperature dependence of the quasielastic scattering in quasicrystals. The general feature of this model is according to equation (5) that both the elastic and the quasielastic intensity vary with Q while the width of the quasielastic peak is constant. The constants C and γ are likely to be temperature dependent. If more than two sites for the jumping atoms are available, $S(Q, E)$ is considerably more complicated than equation (5). This model or a slightly modified one might be used to analyse the present data but as the temperature dependence of $S(Q, E)$ is unknown, such an analysis will not give an unambiguous interpretation.

(3) *Atoms are performing a Brownian motion in a cage.* The case of perfectly reflecting walls of a cage of spherical shape has been treated by Volino and Dianoux [27] and recently generalized by Cvikl *et al* [28] to a cage with partially absorbing walls. In both cases the scattering function consists of a sum of an elastic and a quasielastic component with the latter consisting of the sum of a large number of Lorentzian functions of different widths. The intensity of the elastic peak is controlled by the factor $[3j_1(QR)/QR)]^2$, where R is the radius of the cage. This expression is, for values of QR relevant to our case, a monotonically decreasing function. The quasielastic intensity is correspondingly increasing with Q . However, the most interesting

feature of this model is that it predicts a constant width of the quasielastic peak up to a value of Q which depends on the cage radius. For large Q the width approaches DQ^2 (D is the diffusion constant) as in model (5) below. This model may possibly describe the results but in order to make a proper analysis, data over a larger Q range than presently available are needed.

b. Long-range diffusion

(4) *Atoms are moving via a random-walk process between geometrically equivalent sites in the crystalline lattice.* This case was first treated by Singwi and Sjölander [29] and by Chudley and Elliott [30] and later generalized to include interstitial sites in a bcc lattice by Rowe *et al* [31]. The scattering function is essentially given by

$$S(Q, E) = \mathrm{e}^{-2W}\frac{1}{\pi}\frac{\Gamma(Q)}{E^2+\Gamma(Q)^2} \tag{6}$$

where $G(\boldsymbol{Q})$ depends on $\boldsymbol{Q}$ and on the atomic jump frequency and the jump geometry. The cross section is thus given by a Lorentzian function whose total intensity is varying as e^{-2W} and whose width is oscillating with Q . In the isotropic version of this model which is appropriate to our case $G(\boldsymbol{Q})$ is given by

$$\Gamma(Q) = \frac{\hbar}{\tau}(1 - \frac{\sin(QL)}{QL}) \tag{7}$$

where L is the jump distance and t the residence time. This model does not describe the measured quasielastic scattering satisfactorily.

(5) *Atoms are diffusing in the crystalline lattice as in a continuous medium.* $S(Q, E)$ is in this case is given by equation (6) with $G(\boldsymbol{Q}) = DQ^2$ where D is the diffusion constant. This model does not describe the data.

(6) *Atoms are diffusing according to various point-defect mechanisms.* In this so-called 'encounter' model [32] all interactions between an atom and a particular point defect are taken into account. The scattering function has a form given by equation (6) with $G(\boldsymbol{Q})$ defined by

$$\Gamma(Q) = \frac{\hbar}{\tau_{enc}}[1-h_{enc}(Q)] \tag{8}$$

where τ_{enc} is the mean time between successive encounters of an atom with different point defects. Both τ_{enc} and $h_{enc}(Q)$ depend on the details of the diffusion mechanism. To be applicable to our case $S(Q, E)$ has to be averaged over all directions of $\boldsymbol{Q}$. This model does not describe the data satisfactorily.

In table 3 the characteristic features of the different models are collected as well as the experimental results obtained from the experiments on IRIS and MIBEMOL. In cases where the models predict no elastic scattering, an elastic peak has nevertheless been incorporated as all atoms are not participating in the diffusive motion. Thus, the elastic intensity will vary according to the Debye–Waller factor for the vibrating atoms. It should also be noticed that in all models listed above $\int S(Q, E)\,\mathrm{d}E = \exp(-2W)$. From a comparison of the features of models and experiments it is concluded that the most appropriate model for further analysis is model (1).

7.2. Neutron scattering fundamentals

In order to obtain a firm basis for understanding both the IRIS and the MIBEMOL results and to be able to join them in an appropriate way, we present before entering into discussions, a brief background of neutron scattering fundamentals from an experimental point of view.

Table 3. Characteristic Q dependent features of different models for atomic diffusion in crystalline lattices in the Q range relevant to the experiments in this work.

	Q variation of elastic peak intensity	Q variation of quasielastic peak	
		Intensity	Width
Model 1	oscillating	oscillating	constant
Model 2	oscillating	oscillating	constant
Model 3	monotonously decreasing	continuously increasing	constant, increasing for large Q
Model 4	monotonously decreasing	constant	oscillating
Model 5	monotonously decreasing	constant	continuously increasing
Model 6	monotonously decreasing	constant	oscillating
IRIS experiment at 920 °C	(n–n–n) increasing (n–n–0) decreasing (n–65–0) decreasing	(n–n–n) decreasing (n–n–0) peak at 1.5 Å^{-1} (n–65–0) peak at 1.5 Å^{-1}	for all samples: constant for Q<1.7 Å^{-1}
MIBEMOL experiment at 920 °C	(n–n–n) oscillating (n–n–0) oscillating	(n–n–n) peak at 1.5 Å^{-1} (n–n–0) peak at 1.0 Å^{-1}	(n–n–n) constant (n–n–0) decreasing

It is well known that incoherent scattering probes the dynamics of individual atoms while coherent scattering probes the relative positions of pairs of atoms at different times. In a diffraction experiment where an integration over all energies of the scattered neutrons (hopefully at an almost constant Q) is performed, one is thus getting information on phenomena at a momentary situation in the sample. A measured diffraction pattern, like the ones shown in figure 1, is thus a time average over all the snapshots taken and it yields, via the positions and the intensities of the Bragg peaks, an average distribution of all atoms in the unit cell. The incoherent scattering contributes only to the background.

A measurement of the elastic intensity component eliminates in principle all time-dependent effects, which are due to scattering from thermal displacements from equilibrium positions (phonons). However, the experimental energy resolution ΔE_{res} defines the time interval within which this is valid. The better the resolution the better information one gets on the details of the time-independent disorder in the scatterer, for example time average values of atomic displacements. This does not cause a problem for the data interpretation at low temperatures where the relaxation times for phenomena involving migration of atoms in a crystalline solid are long. It has, however, to be considered when the migration rate of the atoms as well as the relative defect concentration is so large that new long-lived structures might exist from the point of view of coherent scattering. The finite lifetime of a particular configuration of atoms then reveals itself in the width of a diffuse (or equivalently a quasielastic) scattering component. Incoherent elastic scattering gives structural information with regard to the motion of single atoms according to models 1 to 3, discussed above.

The information a quasielastic spectrum contains depends on the energy resolution, ΔE_{res}, of the spectrometer. In order to put numbers in this discussion it is assumed that the smallest broadening of the resolution function, which can be observed, is about $0.5 \cdot \Delta E_{res}$ and the

largest one about $5 \cdot \Delta E_{res}$. The time windows for the IRIS spectrometer is calculated to about $13 \leqslant \tau \leqslant 130$ ps and for MIBEMOL to about $1.3 \leqslant \tau \leqslant 13$ ps. The scattering from any process, which has its relaxation time shorter than the lower limits above, is thus hidden in the phonon background while those with relaxation times longer than the upper limits are hidden in the elastic peak.

Before going further into the interpretation of the results we would like to comment on the measured quasielastic scattering components. In all cases this scattering has been found to be centred around zero neutron energy transfer and it has thus to be considered as really quasielastic and not originating from degenerating optical phonons. This is also corroborated by the fact that the measured diffraction patterns do not reveal any indication of a phase transition in the temperature region 800 to 1000 °C.

7.3. Geometry and relaxation time for atomic jumps

One very specific feature of the elastic peak intensities measured both with high resolution (IRIS) and low resolution (MIBEMOL) from the *n–n–n* sample is that it does not vary with Q according to a Debye–Waller factor but instead is increasing with Q. The intensity does not exhibit any distinct temperature dependence and, furthermore, it is lower than the elastic intensity from the isotope containing samples. The only models which might explain this unusual Q variation are those that assume that atoms perform jumps between different sites in the lattice. Fitting an expression of the type

$$I(Q)_{el} = C_1 + C_2[1 + j_0(Qd)] \tag{9}$$

to the MIBEMOL data obtained at 920 °C a good description of the measured intensities could be obtained (see the full curves in figures 8(a) and 8(b)). The ratio between the values of the fitted curves at $Q = 0$ turns out to be equal to the ratio between the total incoherent scattering cross sections per scattering unit of the two samples which gives, even if the extrapolation from the first experimental point is considerable, both confidence in the applicability of equation (4) and that the measured intensity is mainly of incoherent origin. If the elastic scattering had been of coherent origin to a significant amount, its magnitude would have been substantially affected by replacing the natural Ni by 'zero coherent scattering' Ni. This is not the case. The value of the jump length d was found to be 4.7 Å for the *n–n–n* sample and 2.9 Å for the *n–n–*0 sample. The error in these two values is determined by the positions of the extrema of the fitted curves and it is estimated to be of the order of ± 0.1 Å. Both distances correspond to interstitial positions of octahedral symmetry, i.e. atoms move from interstitial to next-nearest and next-next-nearest substitutional sites and vice versa, in the lattice. The jump to the nearest interstitial position involves a jump length of 2.06 Å. This corresponds to a Q value, which is not possible to reach with the wavelength of the incident neutrons. It should be noted that, as shown in figure 7, the elastic intensity measured at 570 °C is very similar to the one measured at 920 °C, showing that atoms are also jumping at the lower temperature, although at such a slow rate that no quasielastic scattering component is seen. If the atomic jumps are to non-equivalent sites having different potential energy, the parameters C_1 and C_2 in equation (9) are expected to be temperature dependent and, accordingly, also the measured elastic intensity. It can thus be anticipated that atoms are jumping between sites at least approximately equivalent in energy. However, a direct determination of how many sites are involved in the jumping cannot be made as all atoms are not jumping but are vibrating most of the time in more or less permanent positions. Assuming that only two sites are involved the relative values obtained of the constants C_1 and C_2 in equation (9) indicate that about 80% of the atoms contributing to the elastic intensity are jumping. The agreement between the measured data and the expression

gets worse for Q larger than about 2 $Å^{-1}$ which might indicate that the assumption of jumping between equivalent sites is not entirely correct but that the motion is more complex.

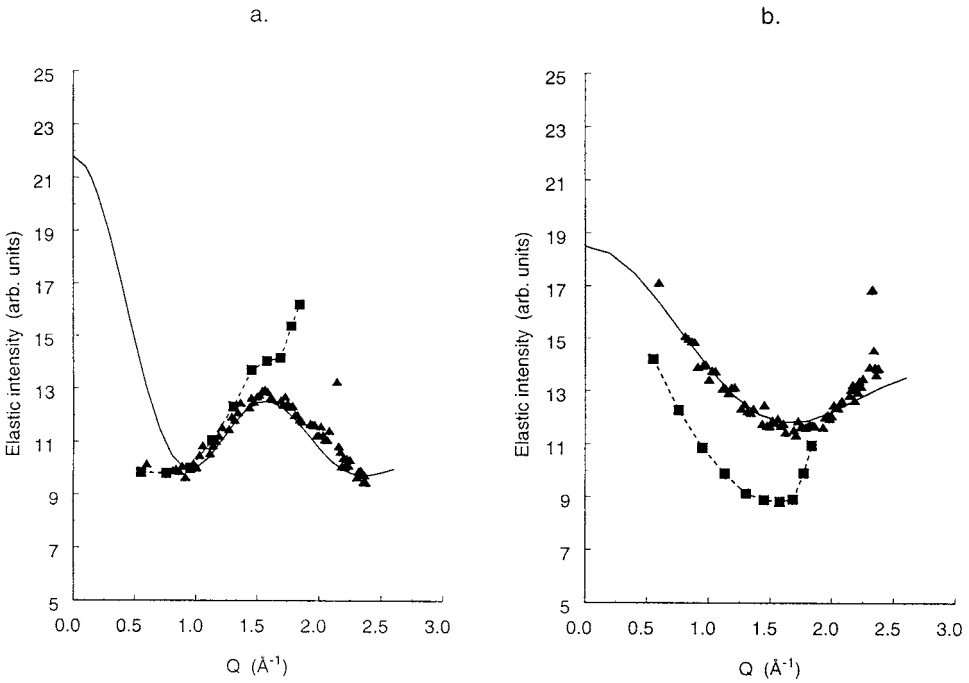

Figure 8. Measured elastic intensities on the MIBEMOL spectrometer. (a) *n–n–n* sample and (b) *n–n–*0 sample. The full curves are fits of equation (9) to the measured points. The points denoted by squares are measured elastic intensities on the IRIS spectrometer. The dotted curve is included to guide the eye.

The elastic intensity measured on the IRIS spectrometer varies qualitatively in the same way as on MIBEMOL (see figure 8). Unfortunately, the amount of vanadium in the calibration sample at the MIBEMOL is not known accurately enough for an absolute normalization. Instead, the two sets of data are normalized to the intensity measured at $Q = 1$ $Å^{-1}$ for the *n–n–n* sample. With this normalization the intensities from the isotope containing samples are considerably lower on IRIS compared to the MIBEMOL ones indicating that the MIBEMOL data contain an intensity component which is quasielastic or even inelastic when observed on IRIS. For Q larger than about 1.6 $Å^{-1}$ the elastic intensities measured on IRIS from all three samples increase dramatically at the same time as the corresponding quasielastic intensities decrease. The increase in elastic intensity cannot be explained in terms of jumping between equivalent sites. The two effects do not cancel in terms of total intensities, which shows that they do not correspond to the same physical phenomenon.

As can be seen in figure 4(d), the elastic intensities, measured on IRIS, from the *n–n–*0 and the *n–*65*–*0 samples have a very similar Q variation. The average of the ratio between the two sets of data is 2.1 ± 0.3, which is somewhat larger than the ratio between the incoherent cross sections of the two samples 1.65. Nevertheless, I_{Cu} can be isolated from the measurements of the two isotopic samples by assuming (i) that the elastic intensity can be written as a sum of two terms, one being the intensity I_{Cu} originating from Cu and one I_{other} including all other scattering contributions and (ii) that I_{Cu} is proportional to the incoherent scattering cross

section (including the self part of the coherent scattering cross section does not make any significant difference for the conclusions below). The result is plotted in figure 9 both for 920 and 570 °C in a logarithmic scale as function of Q^2. If both sets of data are fitted by straight lines, the slopes are found to be 0.35 ± 0.07 and 0.03 ± 0.03 Å^2 at 920 and 570 °C, respectively. In a cubic lattice this corresponds to mean square displacements $\langle u^2 \rangle$ of 1.05 and 0.09 Å^2, showing that Cu atoms have very large motional amplitude at the high temperature. Assuming that $\langle u^2 \rangle$ at 920 °C is determined by atomic jumps between two sites the jump length L is given by $L = (12\langle u^2 \rangle)^{1/2} = 2.05$ Å. This value, as mentioned above, agrees very well with the smallest distance between an atomic and an interstitial position in the $Al_{50}Cu_{35}Ni_{15}$ lattice. Furthermore, the intensity at the smallest Q value is at both temperatures significantly above the fitted line, which is in line with the presence of atomic jumps over larger distances.

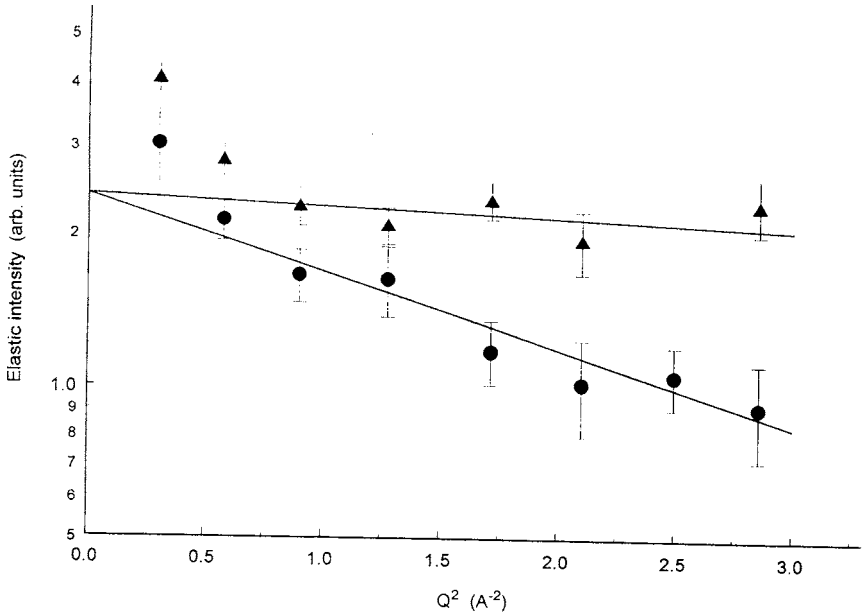

Figure 9. The elastic intensity on MIBEMOL from Cu at 570 (triangles) and 920 °C (circles) plotted in a logarithmic scale as function of Q^2. The lines are obtained by fits of an exponential function.

The measured quasielastic intensity on IRIS can for Q less than about 1.6 Å^{-1} be satisfactorily described by equation (4), the *n*–*n*–*n* sample with a jump length of 4.7 Å and the *n*–65–0, as well as the *n*–*n*–0, samples with a jump length of 2.9 Å (see the full curves in figure 10). For larger Q the intensity drops to very small values. None of the models (1)–(6) above predicts such a behaviour. This is the same Q region where the elastic intensities are increasing as well as the width of the quasielastic peak. As mentioned above, the ratio between the quasielastic intensities for the *n*–65–0 and *n*–*n*–0 samples are found is larger than the ratio between the incoherent scattering cross sections. This indicates that the quasielastic scattering is not fully incoherent but contains some significant amount of coherent origin. Realizing that the two intensity distributions in figure 11 have maxima at Q values close to the $\frac{1}{2}$[110] and $\frac{1}{2}$[200] reciprocal lattice vectors (see figure 1) it can be conjectured that the measured quasielastic scattering, to a substantial part, can be classified as diffuse scattering resulting from a dynamic disorder in a structure twice the size of the direct lattice.

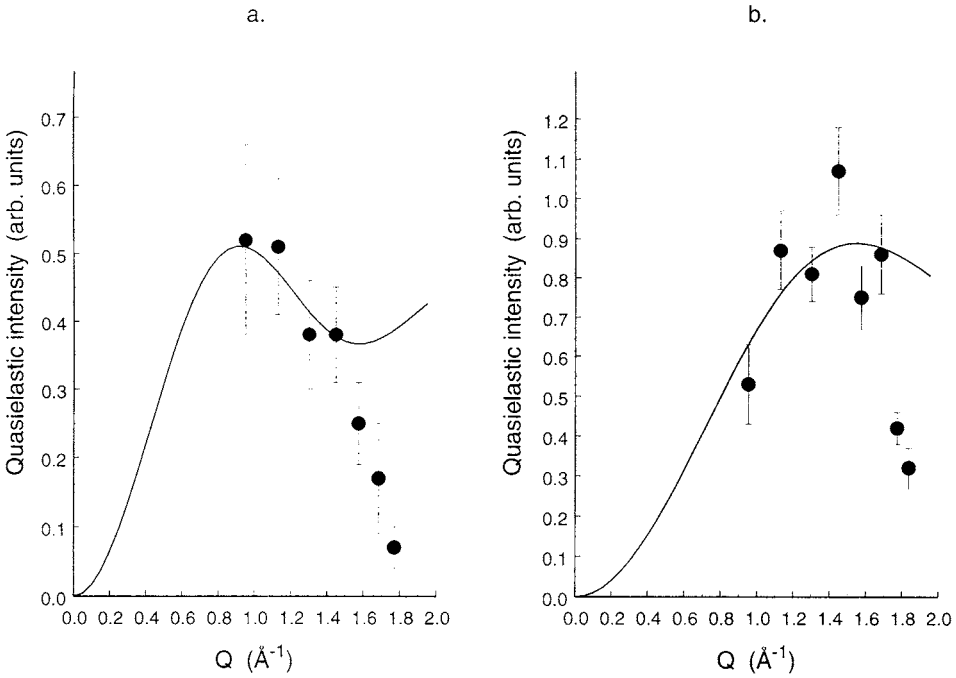

Figure 10. Fits of the second term in equation (4) to measured quasielastic intensities at 920 °C on IRIS. (a) *n*–*n*–*n* sample and (b) *n*–65–0 sample.

Equation (4) contains a quasielastic intensity component whose width gives a value of the residence time of an atom in one site. As can be seen from figure 7 the magnitude of the quasielastic peak on MIBEMOL is about 2% of the elastic one for both the *n*–*n*–*n* and the *n*–*n*–0 samples. As the sum of elastic and quasielastic intensities should vary with Q according to the Debye–Waller factor, it can thus be concluded that the observed quasielastic peaks are not corresponding to the observed elastic intensities in the way predicted by equation (4). This means that G is much larger than the resolution of the MIBEMOL spectrometer and thus the relaxation time t is smaller than about 0.7 ps. The corresponding quasielastic intensities are therefore hidden under the elastic peak and they are not possible to detect within the experimental limits of error. As the Ni atoms have by far the largest incoherent cross section it can be corroborated that they are the ones performing the rapid jump motion with a jump length of about 4.7 Å and on the time scale of less than about 0.7 ps. The 2.7 Å jump has then to be assigned to Al and/or Cu atoms, but from atomic size considerations and from the structure of the $Al_{50}Cu_{35}Ni_{15}$ lattice [23] it is more likely to be Cu atoms. It should be remarked at this point that a collective jump phenomenon with similar characteristic features has been seen in neutron quasielastic scattering measurements on the $Al_{62}Cu_{25.5}Fe_{12.5}$ quasicrystal [10] at 770 °C.

The intensity of the quasielastic peaks in the MIBEMOL spectra also exhibits an oscillating behaviour, which can be described by equation (4). The magnitude of the intensities from the two samples are very similar and agrees within limits of error with the ratio between the incoherent cross sections (see table 1). Thus, assuming that the intensity is of incoherent origin, the expression $C_1 e^{-2W}(1 - j_0(qd))$ was fitted to the measured intensities with $2W = 0.03Q^2$. The agreement is satisfactory (see the full curves in figure 11) and the values obtained for the

jump distance d are the same as those obtained from the elastic intensities. However, in this case the long distance, 4.7 Å, is associated with the *n–n–*0 sample and the short one, 2.9 Å, with the *n–n–n* sample, which is in apparent contradiction to the earlier results. However, this can be resolved by realizing the importance of the time window accessible by the spectrometer used. The width of the quasielastic peaks are within limits of error constant and the residence time of a jumping atom, presumably a Ni atom, in the *n–n–n* sample is found to be 1.3 ps and of a Cu atom in the *n–n–*0 sample 0.95 ps. For both samples the agreement between calculated and measured intensities is poor for Q larger than 2.2 $Å^{-1}$, which might be due to the presence of some other jump length, probably the 2.06 Å jump mentioned above.

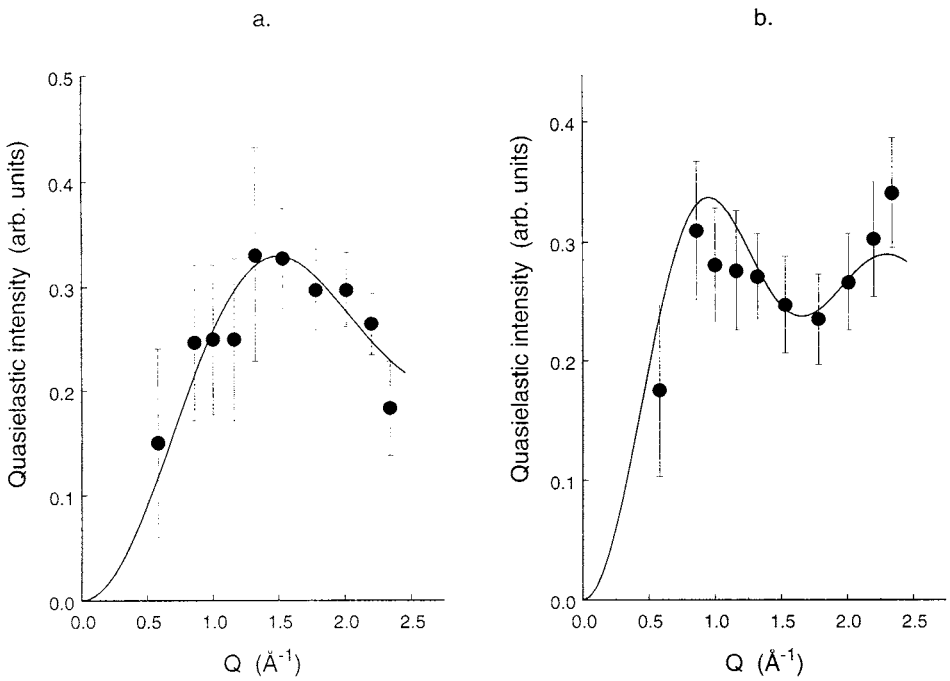

Figure 11. Intensity and FWHM of the quasielastic peak measured on the MIBEMOL spectrometer. (a) *n–n–n* sample and (b) *n–n–*0 sample. The full curves are fits of the second term in equation (4) to the measured points.

The observation that the quasielastic scattering contains a coherent scattering contribution makes it probable that the increase in elastic intensity at large Q also has a coherent origin. As the magnitude of the increase is the same in the *n–n–n* and *n–n–*0 samples but approximately proportional to the Cu coherent cross section, it can be then concluded that this elastic intensity originates from Cu atoms.

The width of the quasielastic scattering, measured on IRIS, is very similar for all three samples. The average value of the width for Q smaller than 1.6 $Å^{-1}$ corresponds to 75 ± 5 ps. For large Q the width is increasing but as the error bars are large no attempt to interpret this behaviour has been made.

8. Conclusions

From the above considerations the following picture of the atomic motions in the $Al_{50}Cu_{35}Ni_{15}$ alloy appears:

- The elastic intensity measured on MIBEMOL shows that atoms are performing rapid jumps between at least two sites at both 570 and 920 °C. The residence time in one position is less than 0.7 ps. The jump lengths involved are 4.7 Å, assigned to Ni atoms and 2.7 Å, assigned to Cu atoms. The distances correspond to jumps between substitutional and next-nearest and next-next-nearest octahedral interstitial positions in the lattice.
- The quasielastic scattering at 920 °C on MIBEMOL indicates the presence of one jump process on the length scale 2.7 Å and relaxation time 1.3 ps, probably to be assigned to Ni atoms, and a further jump process on the length scale 4.7 Å and relaxation time 0.95 ps, probably to be assigned to Cu atoms. At 570 °C, no quasielastic scattering is observed which indicates that the relaxation times at this temperature are outside the time window of both IRIS and MIBEMOL. Apparently, these two jump processes are governed by activation energies.
- The elastic scattering on IRIS reveals that the Cu atoms are also jumping between substitutional and nearest interstitial sites with a residence time less than about 10 ps.
- The quasielastic scattering on IRIS reveals the existence of structures existing long enough to give rise to diffuse coherent scattering. This can be concluded from the fact that the quasielastic intensity is drastically decreasing when Q approaches a reciprocal lattice point. The lifetime of a configuration of atoms on interstitial octahedral sites is of the order of 75 ps. At low temperature no quasielastic scattering is observed within the experimental accuracy. It can thus be concluded that at low temperature the atoms are jumping on an individual basis while with increasing temperature the jumps are more and more correlated. The magnitude of the quasielastic (diffuse) scattering is thus expected to increase with temperature while its width in energy and Q should be relatively temperature independent.
- The Huang scattering present in the diffraction data at high temperatures shows that the atomic jump motions in the lattice create a long-range distortion field in the [200] direction in the crystalline lattice. The associated activation energy is 0.6 eV, which is very close to the activation enthalpy for both vacancy formation and for atomic migration in the aluminium lattice.
- All atomic motions on a time scale up to about 100 ps are local. No sign of the existence of long-range diffusion or of an atomic diffusion process within a cage has been observed. This sets the upper limit for the self diffusion coefficient to about 10^{-7} cm^2 s^{-1}. It should, however, be added that the Q range in the present experiments might have been too small to reveal such a motion.
- Both the space and the time evolvement of the atomic diffusive motions in the ternary $Al_{50}Cu_{35}Ni_{15}$ alloy is very similar to what has been found in ternary alloys with quasicrystalline and quasicrystalline-like local order. From the results presented above it can thus be concluded that frequent atomic jumps between interstitial positions are likely to take place on a picosecond time scale in any alloy above a certain relative vacancy concentration and it is not a characteristic feature of quasicrystals. This is in agreement with findings of Mehrer and coworkers [17, 18]. A general conclusion then is that the mechanism of atomic motions, at least in Al-based ternary compounds, is also independent of their periodic or aperiodic structure.

Acknowledgments

The authors are grateful for the very good help given by Remi Kahn during the measurements on MIBEMOL. They also want to express their thanks to Marc Zandona for making the x-ray checks on the produced samples and to André Simon, director of LSG2M, for providing funds for the purchase of the Cu isotopes.

References

[1] Göltz G, Heidemann A, Mehrer H, Seeger A and Wolf D 1980 *Philos. Mag.* A **41** 723
[2] Vogl G, Petry W, Flottmann Th and Heiming A, 1989 *Phys. Rev.* B **39** 5025
[3] Bée M 1988 *Quasi-Elastic Neutron Scattering* (Bristol: Adam Hilger)
[4] Bocquet J L, Brebec G and Limoge Y 1996 *Physical Metallurgy* ed R W Cahn and P Haasen (Amsterdam: Elsevier) p 535
[5] Kalugin P A and Katz A, 1993 *Europhys. Lett.* **21** 921
[6] Coddens G, Bellissent R, Calvayrac Y and Ambroise J P 1991 *Europhys. Lett.* **16** 271
[7] Coddens G, Lyonnard S and Calvayrac Y 1997 *Phys. Rev. Lett.* **78** 4209
[8] de Araújo J H, Gomes A A and da Cunha J B M 1996 *Solid State Commun.* **97** 1025
[9] Lyonnard S, Coddens G, Calvayrac Y and Gratias D 1996 *Phys. Rev.* B **53** 3150
[10] Coddens G 1997 *Int. J. Mod. Phys.* B **11** 1679
[11] Dolinšek J, Ambrosini B, Vonlanthen P, Gavrilano J L and Chernikov M A 1998 *Phys. Rev. Lett.* **81** 3671
[12] Lu S S and Chang T 1957 *Acta Phys. Sinica* **13** 150
[13] Van Sande M, de Ridder R, Van Landuyt J and Amelinckx S 1978 *Phys. Status Solidi* a **50** 587
[14] Chattopadhyay K, Lele S, Thangaraj N and Ranganathan S 1987 *Acta Metall.* **35** 727
[15] Würschum R, Troev T and Grushko B 1995 *Phys. Rev.* B **52** 6411
[16] Kanazawa I, Hamada E, Saeki T, Sato K, Nakata M, Takeuchi S and Wollgarten M 1997 *Phys. Rev. Lett.* **79** 2269
[17] Zumkley Th, Mehrer H, Freitag K, Wollgarten M, Tamura N and Urban K 1996 *Phys. Rev.* B **54** R6815
[18] Mehrer H, Zumkley Th, Eggersmann M, Galler R and Salamon M 1998 *Mat. Res. Soc. Symp. Proc.* **527** 3
[19] He L X, Wu Y K and Kuo K H 1988 *J. Mater. Sci. Lett.* **7** 1284
[20] Zhang H and Kuo K H 1989 *Scripta Met.* **23** 355
[21] Villars P, Prince A and Okamoto H (eds) 1995 *Handbook of Ternary Phase Diagrams, ASM International* Vol 3
[22] Krivoglaz M A 1996 *X-ray and Neutron Diffraction of Nonideal Crystals* (Berlin: Springer)
[23] Wollenberger H J 1996 *Physical Metallurgy* ed R W Cahn and P Haasen (Amsterdam: Elsevier) p 1622
[24] Teatum E T, Gschneidner K A Jr and Waber J T 1968 *Report LA-4003, UC-25, Metals, Ceramics and Materials, TID-4500* Los Alamos Scientific Laboratory, cited in
Ferro R and Saccone A *Physical Metallurgy* ed R W Cahn and P Haasen (Amsterdam: Elsevier) p 206
[25] Schober H R, Petry W and Trampenau J 1993 *J. Phys.: Condens. Matter* **4** 9321
[26] Sivia D S, Carlile C J, Howells W S and König S 1992 *Physica* B **182** 341
[27] Volino F and Dianoux A J 1980 *Molec. Phys.* **41** 271
[28] Cvikl B, Dahlborg U and Calvo-Dahlborg M 2000 *Proc. Int. Conf. on Nuclear Energy in Central Europe '99, 6-9 September 1999, Portoro, Slovenia* at press
[29] Singwi K S and Sjölander A 1960 *Phys. Rev.* **119** 1093
[30] Chudley G T and Elliott R J 1961 *Proc. Phys. Soc.* **77** 353
[31] Rowe J M, Sköld K, Flotow H E and Rush J J 1971 *J. Phys. Chem. Solids* **32** 41
[32] Wolf D 1977 *Solid State Commun.* **23** 853
Wolf D 1983 *Philos. Mag.* **47** 147